01 Jun 2013

Characterisation of Ga2O3-Na2O-CaO-ZnO- SiO2 Bioactive Glasses

A. W. Wren

T. Keenan

A. Coughlan

F. R. Laffir

et. al. For a complete list of authors, see https://scholarsmine.mst.edu/che_bioeng_facwork/1145

Recommended Citation

A. W. Wren et al., "Characterisation of Ga2O3-Na2O-CaO-ZnO- SiO2 Bioactive Glasses," *Journal of Materials Science*, vol. 48, no. 11, pp. 3999 - 4007, Springer, Jun 2013.
The definitive version is available at https://doi.org/10.1007/s10853-013-7211-2

J Mater Sci (2013) 48:3999–4007
DOI 10.1007/s10853-013-7211-2

Characterisation of Ga_2O_3–Na_2O–CaO–ZnO–SiO_2 bioactive glasses

A. W. Wren · T. Keenan · A. Coughlan · F. R. Laffir · D. Boyd · M. R. Towler · M. M. Hall

Received: 24 July 2012 / Accepted: 31 January 2013 / Published online: 12 February 2013

Abstract The structural role of Gallium (Ga) is investigated when substituted for Zinc (Zn) in a $0.42SiO_2$–0.40–xZnO–$0.10Na_2O$–0.08CaO glass series, (where $x = 0.08$). Each starting material was amorphous, and the network connectivity (NC) was calculated assuming Ga acts as both a network modifier (1.23), and also as a network former. Assuming a network forming role for Ga the NC increased with increasing Ga concentration throughout the glass series (*Control* 1.23, *TGa-1* 2.32 and *TGa-2* 3.00). X-ray photoelectron spectroscopy confirmed both composition and correlated NC predictions. Raman spectroscopy was employed to investigate Q-structure and found that a shift in wavenumbers occurred as the Ga concentration increased through the glass series, from 933, 951 to 960 cm^{-1}. Magic angle spinning nuclear magnetic resonance determined a chemical shift from −73, −75 to −77 ppm as the Ga concentration increased, supporting Raman data. These results suggest that Ga acts predominantly as a network former in this particular Zn-silicate system.

A. W. Wren (✉) · T. Keenan · A. Coughlan · M. R. Towler · M. M. Hall
Inamori School of Engineering, Alfred University, Alfred, NY 14802, USA
e-mail: wren@alfred.edu

F. R. Laffir
Materials and Surfaces Science Institute, University of Limerick, Limerick, Ireland

D. Boyd
Department of Applied Oral Sciences, Dalhousie University, Halifax, NS, Canada

M. R. Towler
Department of Biomedical Engineering, University of Malaya, Kuala Lumpur, Malaysia

Introduction

Glass-based biomaterials are playing an increasing role in orthopaedics and reconstructive surgery as they can incorporate ions that have a therapeutic effect in vivo. These materials include bioactive glasses (Bioglass) which are employed as bone void fillers in either particulate or paste form [1]. Bioglass based glass/ceramic scaffolds [2–6] and polymer/bioglass composites [7–9] encourage cell proliferation and differentiation upon implantation into the body [3, 10]. For the work contained herein Gallium (Ga) was added to a bioactive glass formulation as it is known to have therapeutic medical potential. Previous work has demonstrated the efficacy of Ga against opportunistic pathogenic bacteria, such as *Pseudomonas aeruginosa* which can cause airway infections in cystic fibrosis patients [11–14], and opportunistic fungi such as *Cryptococcus neoformans*, which can cause life threatening diseases in immuno-compromised patients [15]. Ga has also been investigated as chemotherapeutics [16]. Numerous compounds such as Ga-chloride, Ga-nitrate, Ga-maltolate, doxorubicin-Ga-transferrin conjugates have been investigated [16]. Previous work on Ga-containing phosphate-based glasses has been conducted by Valappil et al. [11], however that study focused on determining the antimicrobial properties.

One of the most important characteristics attributed to bioactive glasses is the rate of dissolution when immersed in an aqueous medium, such as human plasma, for prolonged periods of time [17–19]. It is known that the partial dissolution of the glass particles surface results in the formation of a silica-rich gel layer and subsequently the precipitation of a calcium phosphate layer [1]. Silicate-based bioactive glasses include network modifiers (Ca^{2+}, Na^{+}, K^{+}) to disrupt the continuity of the Si–O–Si bonds within the glass leading to

the formation of non-bridging oxygen groups (Si–O–NBO) [17]. The presence of NBO groups facilitates the ion exchange process and as the concentration of alkali/alkali earth cations increases, the higher rate of silica dissolution further increases bioactivity [17]. An important consideration when designing bioactive glasses is to determine the role of additional elements on glass chemistry. Elements such as aluminium (Al) have been widely studied regarding glass chemistry as it can act as a network former in glass melts where it exists in four-fold coordination (AlO_4 tetrahedra) where charge compensation is provided by alkali cations. Both Al and Ga are Group III elements where Ga is located directly below Al in the periodic table [20]. Property measurements on alkali gallio-silicate glasses indicate that Ga effectively performs a similar role as Al in comparable glass compositions [20]. Previous studies by Baker et al. [21] have substituted Al^{3+} with Ga^{3+} as their role in silicate glasses has been shown to be identical by Raman studies of alumino-silicate and gallio-silicate glasses. Determining a bioactive glass network former such as Ga^{3+} may be beneficial there are many negative attributes associated with Al^{3+} in bioactive materials including neurotoxicity [22] and inhibition of apatite crystallisation [23].

The study undertaken herein looks to determine the structural role of Ga when substituted for zinc (Zn) in a SiO_2–CaO–Na_2O_3–ZnO/Ga_2O_3 series of bioactive glasses. Zn has previously been identified as acting predominantly as a network modifier in similar glasses [24]. Traditional methods for analysis of vitreous materials have been employed including Raman spectroscopy, X-ray photoelectrons spectroscopy (XPS) and magic angle spinning nuclear magnetic resonance (MAS-NMR).

Experimental

Synthesis

Three glasses were formulated for this study, two Ga-containing glasses (*TGa-1*, *TGa-2*) and a Ga-free CaO–Na_2O–ZnO–SiO_2 glass (*Control*). *TGa-1* and *TGa-2* contain incremental concentrations of Ga_2O_3 at the expense of ZnO. Glass compositions (mol. fr., see Table 1) were prepared by two methods described in Sect. 2.2.

Sample preparation

Glass powder production

The powdered mixes of analytical grade reagents (Fisher Scientific, PA, USA) were oven dried (100 °C, 1 h) and fired (1500 °C, 1 h) in platinum crucibles and shock quenched in water. The resulting frit were dried, ground and sieved to retrieve glass powders with a maximum particle size of 90 μm.

Table 1 Glass compositions (mol. fr.) and composition determined by XPS

	Control	*TGa-1*	*TGa-2*
SiO_2	0.42 (0.45)	0.42 (0.45)	0.42 (0.46)
Ga_2O_3	0.00 (0.00)	0.08 (0.05)	0.16 (0.10)
ZnO	0.40 (0.35)	0.32 (0.28)	0.24 (0.21)
Na_2O	0.10 (0.10)	0.10 (0.12)	0.10 (0.12)
CaO	0.08 (0.11)	0.08 (0.11)	0.08 (0.10)

Glass rod production

The powdered mixes of analytical grade reagents (Fisher Scientific, PA, USA) were oven dried (100 °C, 1 h) and fired (1500 °C, 1 h) in platinum crucibles. Glass castings were produced by pouring the melts into graphite moulds which were preheated to T_g −20 °C. The graphite moulds were left for 1 h and furnace cooled in order to anneal the glass. The resulting glass casts were then sectioned with a diamond blade on an Isomet 5000 Linear Precision Saw (1500 rpm, 0.4 mm min^{-1}) and were shaped into approximate dimensions of 15 × 3 × 3 mm using a Phoenix 4000 grinding machine with 60-μm silicon carbide grinding paper (Buehler, IL, USA).

Glass characterisation

X-ray diffraction (XRD)

Diffraction patterns were collected using a Siemens D5000 X-ray Diffraction Unit (Bruker AXS Inc., WI, USA). Glass powder samples were packed into standard stainless steel sample holders. A generator voltage of 40 kV and a tube current of 30 mA was employed. Diffractograms were collected in the range $10° < 2\theta < 80°$, at a scan step size 0.02° and a step time of 10 s.

Particle size analysis (PSA)

Particle size analysis was achieved using a Beckman Coulter Multisizer 4 Particle size analyzer (Beckman-Coulter, Fullerton, CA, USA). Glass powder samples were evaluated in the range of 0.4–100.0 μm with a run length of 60 s. The fluid used was de-ionized water at a temperature range between 10 and 37 °C. The relevant volume statistics were calculated on each glass.

X-ray photoelectron spectroscopy (XPS)

X-ray Photoelectron Spectroscopy (XPS) was performed in a Kratos AXIS 165 spectrometer (Kratos Analytical,

Manchester, UK) using monochromatic Al Kα radiation ($h\upsilon = 1486.6$ eV). Glass rods with dimensions of 15 × 3 × 3 mm were produced from the melt and fractured under vacuum ($\sim 2 \times 10^{-8}$ torr) to create pristine surfaces with minimum contamination. Surface charging was minimised by flooding the surface with low energy electrons. The C 1*s* peak of adventitious carbon at 284.8 eV was used as a charge reference to calibrate the binding energies. High resolution spectra were taken at pass energy of 20 eV, with step size of 0.05 eV and 100 ms dwell time.

Network connectivity (NC)

The NC of the glasses was calculated with Eq. 1 using the molar compositions of each glass. NC calculations were performed assuming that Ga performs as a network former where charge compensation is provided in the order $Na^+ > Ca^{2+}$. Calculations were also conducted assuming Ga acts as a network modifier where 1 mol% Na_2, and 1 mol% Ca forms one NBO group.

$$\mathrm{NC} = \frac{\text{No. BOs} - \text{No. NBOs}}{\text{Total No. Bridging Species}} \quad (1)$$

where:

BO Bridging oxygens
NBO Non-bridging oxygens

Differential thermal analysis (DTA)

A combined differential thermal analyser-thermal gravimetric analyser (DTA-TGA) (SDT 2960 Simultaneous DSC-TGA, TA Instruments, DW, USA) was used to measure the glass transition temperature (T_g) for both glasses. A heating rate of 20 °C min^{-1} was employed using an air atmosphere with alumina in a matched platinum crucible as a reference. Sample measurements were carried out every 6 s between 30 and 1300 °C.

Raman spectroscopy

Raman spectra were collected on glass frit samples using a DILOR XY Labram (Horiba Jobin-Yvon Inc., NJ, USA) with a He–Ne 20 mW laser under a tension of 7.45 mA. A grating number of 1800 was used in association with a Peltier cooled CCD detector and the system was coupled to a confocal microscope Olympus model BX40. Gaussian line shapes were fitted using Fityk analysis software under a number of conditions by previous work by Mysen et al. [25]. Peaks were initially identified using the *Control* glass which presented a clear shoulder at lower wavenumbers which are obvious deviations from the Gaussian line shapes. Additional conditions include that all spectra were considered to have a horizontal background and all spectral bands were considered symmetric.

Magic angle spinning nuclear magnetic resonance (MAS-NMR)

^{29}Si magic angle spinning (MAS) NMR studies were carried out on a Bruker Avance NMR spectrometer with a 9.4T magnet (400.24 MHz proton Larmor frequency, 79.51 MHz ^{29}Si Larmor frequency) using a probe head for 7-mm rotor diameters. The specimens (<45 μm) were spun at 5.00 kHz. 200 scans were accumulated with single pulse excitation using a pulse length of 80° at 28 kHz rf field strength. The recycle delays were chosen to be three times the spin lattice relaxation times as determined by inversion recovery sequences. Spin lattice relaxation times ranged between 15 and 26 s. The chemical shift scale was referenced externally against Kaolin as secondary chemical shift standard at −91.34 ppm (centre between doublet).

Results and discussion

This study was undertaken in order to determine the effect of gallium addition on the structure of SiO_2–ZnO–Na_2O–CaO-based glasses. This glass series was developed as Ga is known to have beneficial effects in vivo with respect to eradicating tumour cells and opportunistic bacteria that may potentially be present in bone defects. In particular, this glass series was developed as a bone void filler as surgical resection of osteosarcoma can leave a population of residual tumour cells in the bone cavity that have the potential to proliferate causing secondary tumours. Bioactive Ga-containing glasses can be used to fill this cavity through an appropriate delivery mechanism. This can include a thermodynamically stable, insoluble hydrogel [26], as these materials are injectable, and can deliver these glass particles which have the potential to eradicate any residual tumour cells. Hydrogels are a suitable candidate as they have a number of desirable properties including the potential to absorb fluid and swell in an aqueous environment which can fill irregular defects [26, 27]. This swelling behaviour can be used to deliver Ga-ions to the entire volume of the surgical cavity. Hydrogels can contain up 95 % water [26], which is the catalyst for bioactive glasses therapeutic effect. They are also considered biocompatible and can be designed to biodegrade over time [26]. However, it is known that the ion release and dissolution of bioactive glasses is dependent on the composition and structural arrangement of the glass network. In particular, the relative fraction of network forming to network modifying cations [17] may significantly augment network dissolution kinetics in the physiological environment.

Traditionally, Ga exists as a trivalent cation (Ga^{3+}) similarly to Al^{3+} and previous studies have used Ga^{3+} as an analogue for Al^{3+} as network formers in glass melts [21]. In the case of alumino-silicate glasses, aluminium (Al) can act as either a network former or modifier. Al^{3+} is able to replace Si^{4+} in the glass network, however, this substitution requires charge balancing cations (Na^+, Ca^{2+}) in order to maintain a neutral charge [28]. Therefore an alumino-silicate glass structure can be regarded as a chain of linked SiO_4 and AlO_4 tetrahedra (assuming the Al/Si ratio $\leq$1/1) [28]. Beyond the ratio of 1/1 Al^{3+} will become a five or sixfold coordination and behave as a network modifier which causes a greater degree of disorder within the glass network [29]. This work employs methods to determine whether Ga^{3+} acts as a network former or modifier in a series of SiO_2–ZnO–Na_2O–CaO bioactive glasses where the Ga_2O_3 substitutes for ZnO in the glass network.

Initial testing includes XRD, which confirmed that each material (*Control*, *TGa-1* and *TGa-2*) produced was amorphous (Fig. 1a). Particle size analysis confirmed similar particle sizes for each glass was used for techniques requiring powdered samples. The mean particle sizes were 11, 10 and 10 μm for *Control*, *TGa-1* and *TGa-2* respectively (Fig. 1b).

In order to confirm the composition and the NC calculations, compositional data was obtained from XPS. Table 1 show the composition of the glass series and the composition as determined by XPS. XPS survey spectra from the *Control* glass is presented in Fig. 2a and identifies the elements Si, O, Ca, Zn, Na and C. C was detected in minimal concentrations between 1 and 3 at.% in the vacuum-fractured surfaces. Figure 2b, c representing survey spectra from *TGa-1* and *TGa-2* were found to contain all the elements present in the *Control* (Si 2*p*, O 1*s*, Ca 2*p*, Zn 2*p* and Na 1*s*) with the addition of Ga. Regarding *TGa-2*, the peak intensity of Ga 2*p* was found to be greater than the *TGa-1* peak intensity. Also the Zn 2*p* peak intensity is found to decrease throughout the glass series as the Ga 2*p* peak intensity increases. XPS compositional data further confirms the original batch compositions presented in Table 1.

NC calculations were conducted assuming that Ga acts as both a network modifying ion and also as a network forming ion. Figure 3a shows the NC calculations assuming that if Ga is acting as a network modifier the NC of each glass composition (*Control, TGa-1*, *TGa-2*) attains a NC of 1.23. Assuming Ga acts as a network former, with Na providing charge compensation, the NC was calculated as 1.23 (*Control*), 2.32 (*TGa-1*) and 3.00 (*TGa-2*). An accepted way to represent the structural arrangement or NC of the constituents of a glass in terms of structural units can be represented by Q^n units, where Q represents the Si tetrahedral unit and *n* the number of bridging oxygens (BO); *n* ranges between 0 and 4 [30]. Si is the central tetrahedral atom which ranges from Q^0 (orthosilicates) to Q^4 (tectosilicates) and Q^1, Q^2 and Q^3 structures representing intermediate silicates containing modifying oxides [30]. The NC calculations presented here (Fig. 3a) predict, that assuming a network forming role, the Q-structure will be approximately Q^2/Q^3 for *TGa-1* (NC = 2.32) and *TGa-2* (NC = 3.00). Assuming a modifying role, the Q-structure will be predominantly Q^1/Q^2 irrespective of Ga concentration, where the NC = 1.23 for *Control*, *TGa-1* and *TGa-2*. The XPS data show similar compositions to the original glass melt formulations. In order to confirm the NC calculations, NC values were re-calculated with the compositional data derived from the XPS. From Fig. 3b, it is evident that assuming Ga acts as a network former, the NC increases from 1.51 to 2.16 (Q^1/Q^2) and 2.82 (Q^2/Q^3) for *Control*, *TGa-1* and *TGa-2* respectively, a trend similar to that observed with the original NC calculations.

Differential thermal analysis (DTA) was used to detect any changes in the T_g as a result of the incorporation of Ga (Fig. 4). In this instance a shift in T_g can indicate that structural changes are occurring within the glass as the concentration of Ga is increased. Regarding the shift in T_g in this instance (561 °C—*Control*, to 569 °C—*TGa-1*, to 587 °C—*TGa-2*), the T_g was found to increase as the concentration of Ga is increased in the glass melt from 0 mol% (*Control*) to 8 mol% (*TGa-1*) to 16 mol% (*TGa-2*), respectively. This shift suggests increased glass stability, which may be attributed to the formation of BO groups. Previous work by the authors on TiO_2 containing bioactive glass shows that a reduction in T_g is indicative of depolymerisation of the glass network (Si–O–Si bonds) as a function of increased network modifier concentration [31]. This work contrasts these previous findings where the T_g increased, indicating that the addition of Ga may promote the formation BO species which likely exist as Si–O–Ga groups formed in the glass.

High resolution XPS spectra of oxygen (O 1*s*) and silica (Si 2*p*) were obtained to determine the effect of Ga substitution. The O 1*s* (Fig. 5a) shows that the binding energy (BE) of the *Control* and *TGa-1* was 530.6 eV while the BE of *TGa-2* experienced a shift to a higher BE of 530.8 eV. The O 1*s* peaks are broad with a FWHM (full width at half maximum) of peaks at $\sim$1.8 eV suggesting a multi local environment of the oxygen atoms in terms of BO and NBO species. NBO groups (Si–O–NBO) are known to disrupt the glass network by depolymerising the Si–O–Si bonds [31]. This is regarded as a positive attribute as this facilitates the ion exchange process which in turn increases bioactivity of these materials [17, 30]. Regarding this work, the O 1*s* of *TGa-1* shifted to a higher BE which is indicative of increasing the BO content in the glass, further suggesting that Ga acts as a network former in these glasses. Figure 5b

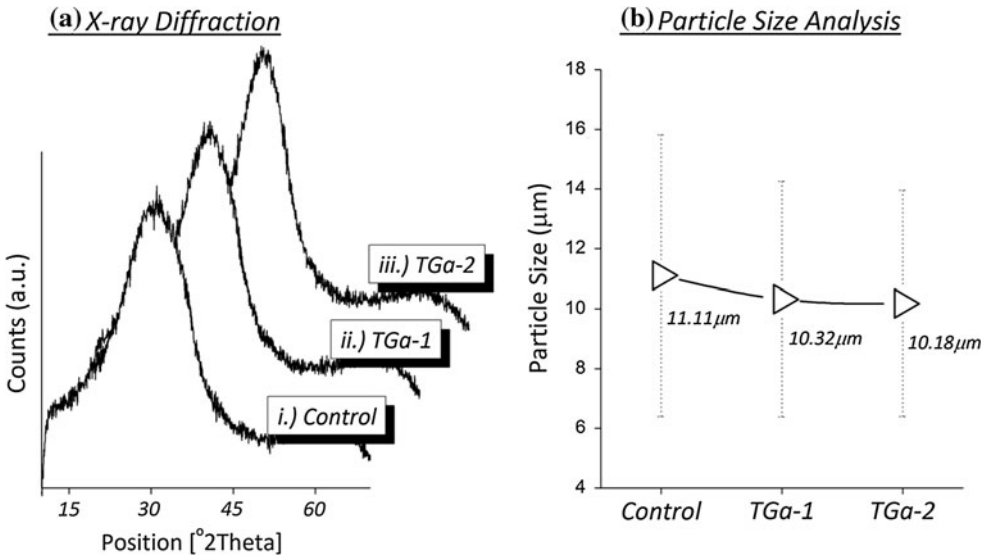

Fig. 1 **a** X-ray diffraction and **b** particle size analysis of *Control*, *TGa-1* and *TGa-2*

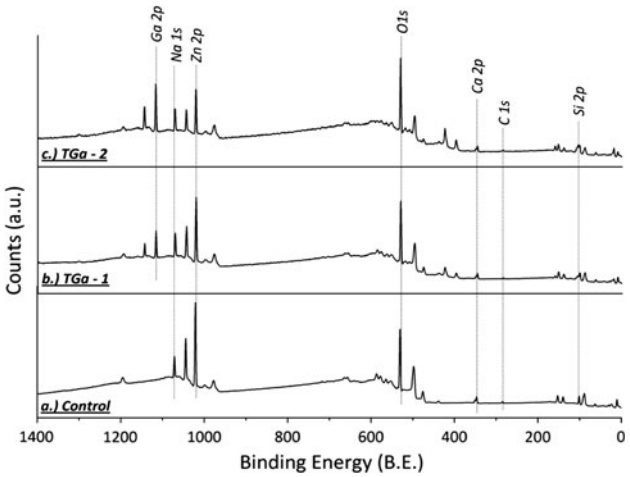

Fig. 2 XPS survey scan of **a** *Control*, **b** *TGa-1* and **c** *TGa-2*

shows Si 2*p* high resolution XPS data. The BE of Si 2*p* was found to be 101.7 eV for each glass (*Control*, *TGa-1* and *TGa-2*). The overlapping doublet peaks at higher BE in Fig. 5b is associated with Ga 3p. The relevant BE are presented for each element in Table 2. Na 1 s was found to shift from 1070.8–1071.3 eV. Zn 2*p* exhibited a slight shift to a higher BE 1021.0–1021.4 eV. Ca 2*p* remained at 347.1 eV regardless of Ga concentration. Increasing the concentration of Ga also exhibited a slight shift from a lower to a higher BE for Ga 2*p* from 1117.0 to 1117.3 eV.

Raman spectroscopy was employed in order to further investigate the glass structure. Raman has previously been used to investigate the Q-structure and to detect local defects in glass structure created by the addition of network modifying oxides [30, 32]. Raman shifts have been assigned based on the connectivity of Si to oxygen in the glass structure where 4-NBO/Si is present at 850 cm^{-1} (Q^0), 3 NBO/Si at 900 cm^{-1} (Q^1), 2-NBO/Si at 1000–950 cm^{-1} (Q^2), 1-NBO/Si at1100–1050 cm^{-1} (Q^3) and a fully polymerised tetrahedral network (Q^4) is a result of asymmetric Si–O stretching vibrations at 1200 cm^{-1} [25, 33]. Figure 6a represents the *Control* glass which presents the most intense band visible at 933 cm^{-1} with a shoulder at 858 cm^{-1}. Previous Raman studies found that the region 950–1000 cm^{-1} is indicative of Si–O–NBO stretching vibration where 2-NBO groups exist per SiO_4 tetrahedron which can be represented as Q^2-structure [25]. The band present at 858 cm^{-1} is associated with 4-NBO/Si, which is typical of a highly disordered glass structure [25]. Broadening of the spectral envelope at lower wavenumbers is indicative of increased network disruption. It is evident from Fig. 6 that as the Ga concentration in the glass increases, the shoulder present at the lower wavenumbers diminishes, particularly at the higher Ga concentrations (16 mol%). Broadening of the spectral envelope to higher wavenumbers reveals the presence of structural units with a higher Q-structure. The peak at 1017 cm^{-1} can be associated with Q^2/Q^3 as it lies close to the Q^3 range of 1050–1100 cm^{-1}. Q^3 indicates the presence of 3-BO groups per SiO_4 tetrahedron [33]. *TGa-1* (Fig. 6b) shows the presence of the main band at 951 cm^{-1} with a shoulder at 869 cm^{-1}. The band intensity at 869 cm^{-1} is reduced with the addition of Ga to the glass. Similarly to the *Control* glass the band at 951 cm^{-1} represents Si–O–2NBO where the band at 869 cm^{-1} represents 4-NBO/Si [25]. The band present at 1040 cm^{-1} represents higher structural units such as Q^3. Figure 6c shows the spectral envelope for *TGa-2* where, similarly to *TGa-1*, there is a shift to higher wavenumbers for each of the peaks identified. There is also a reduction in the intensity of the shoulder present (particularly when compared to the *Control*) at lower wavenumbers. The main band associated with *TGa-2* is centred at 960 cm^{-1} which is shifted to higher wavenumbers when compared to *Control* (933 cm^{-1}) and *TGa-1* (951 cm^{-1}).

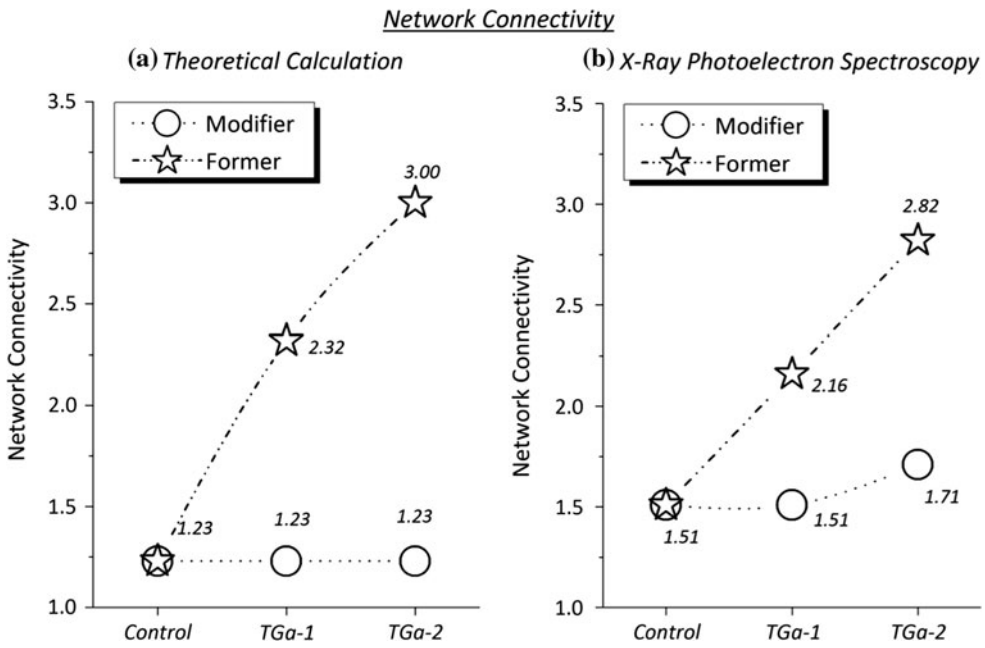

Fig. 3 Network connectivity of Ga-glass series based on **a** theoretical calculations and **b** XPS data

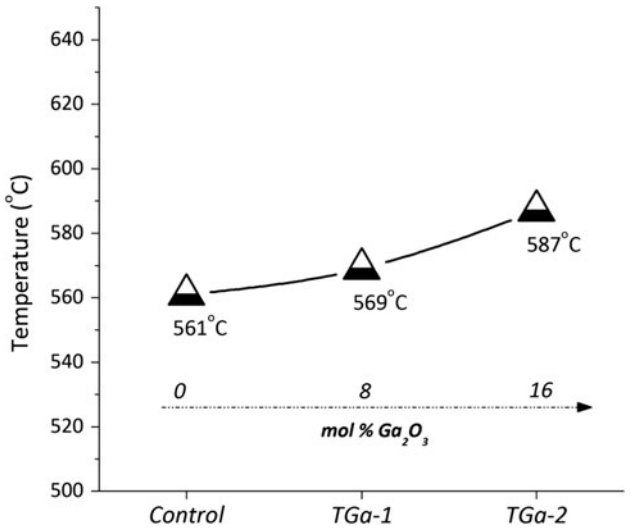

Fig. 4 Glass transition temperatures of Ga-glass series

Also the intensity of the peak at the lower wavenumbers (883 cm^{-1}) is greatly reduced when compared to *Control* (858 cm^{-1}) and is shifted to higher wavenumbers. The intensity of the peaks at higher wavenumbers (1042 cm^{-1}), i.e. Q^3-structures, is also higher in intensity and in wavenumbers location than both *Control* and *TGa-1*, suggesting greater connectivity within the glass network.

The data generated from Raman spectroscopy correlates with NC calculations (assuming Ga acts as a network former) where *Control* has predominantly Q^1/Q^2 structure, *TGa-1* has predominantly Q^2-structure and *TGa-2* has a Q^2/Q^3 structure. Raman assignments and Q-structures in $CaSiO_2$ and $NaAlSiO_4$ melts have previously been identified by Mysen et al. which identified asymmetric stretching modes for the regions 850–880 cm^{-1} (4-NBO/Si), 900–920 cm^{-1} (3-NBO/Si), 950–980 cm^{-1} (2-NBO/Si) and 1050–1100 cm^{-1} for 1-NBO/Si. Fully polymerised Si–O–Si (Q^4) structures, with 0-NBO/Si were assigned to having anti-symmetric stretch mode at 1060 and 1190 cm^{-1}. It is likely that the spectral envelopes presented here include a distribution of Q^n species with the spectral shifts representing the predominant Q^n species present in the glass. Previous work by Branda et al. [34] identified Ga as acting as a network former, and having an analogous role to Al^{3+} in glass melts and that these M^{3+} reduces the in vitro bioactivity. Although the general consensus is that the formation of NBO in bioactive glasses is essential to bioactivity and ion exchange [17], bioactive elements included in network forming roles can play an essential role where their incorporation can further control the glass degradation rate and ion exchange process.

MAS-NMR was employed to further investigate the structural effects of Ga incorporation. Chemical shift in MAS-NMR represents structural changes around the Si atom which lies in the region of −60 to −120 ppm for SiO_4 tetrahedra [35]. Figure 7 shows the chemical shift relating to *Control*, *TGa-1* and *TGa-2* as the Ga concentration in the glass increases from 0, 8 to 16 mol% respectively. Peaks were identified at −73.97 ppm (*Control*) to −75.81 ppm (*TGa-1*) to −77.50 ppm (*TGa-2*). From Fig. 7, it is evident that a higher fraction of Q^0 and Q^1 species exist in the *Control* glass. The shoulder located at between −60 and −70 ppm decreases when observing *TGa-1* and *TGa-2*. This is indicative of greater network disruption where Q^0 and Q^1 represents 4-NBO/Si and 3NBO/Si, respectively [36]. The observed shift in ppm

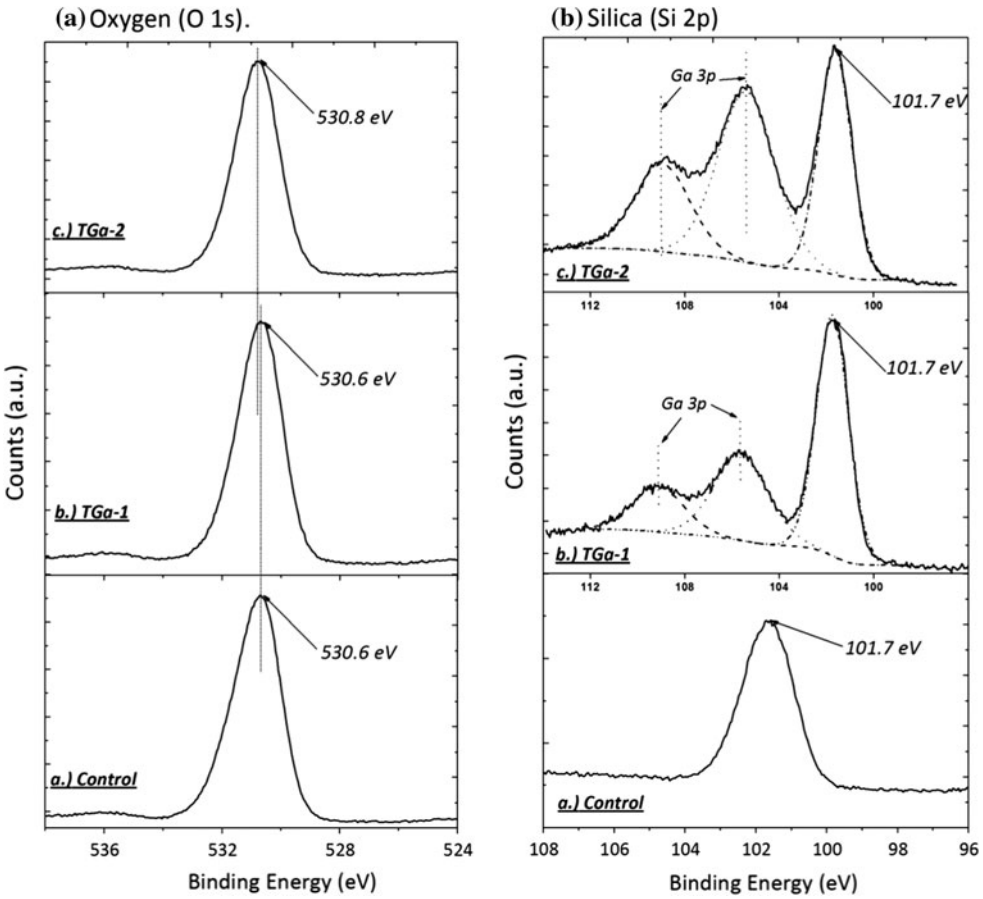

Fig. 5 High resolution XPS, **a** O 1*s* and **b** Si 2*p* of Ga-glass series

Table 2 Binding energies of elements determined by XPS

	Na 1*s* (eV)	Zn 2*p* (eV)	Ca 2*p* (eV)	Ga 2*p* (eV)
Control	1071.3	1021.4	347.1	–
TGa-1	1070.8	1021.0	347.1	1117.0
TGa-2	1071.2	1021.2	347.1	1117.3

with the addition of Ga indicates that a higher concentration of BO's is present. The *Control*, with a chemical shift of −73.50 ppm correlates with NC and Raman studies where the peak lies between Q^1/Q^2 structural units, suggesting a predominantly Q^1 orientated network. However Q^0, Q^2 and Q^3 species are also present as evinced by the broadening of the spectral envelope. Regarding *TGa-1* the peak centres at −75.81 ppm which is just below the centre for Q^2 species (−77 ppm). This also suggests predominantly Q^2 structure, however, the Q^1 and Q^3 shoulders contribute significantly to the structure. Q^3 species in this instance are more prominent when compared to the *Control* glass. *TGa-2* exhibited a peak centred at −77.50 ppm which represent Q^2 species, however, the shoulder representing Q^3 species is much more prominent than either the *Control* or *TGa-1* suggesting a higher degree of order within the glass network, which may be attributed to the presence of BO's groups which are formed as Si–O–Ga bridges, where the Ga structures are charge compensated by Na. The spectral band of each glass was found to contain a number of Q^n species, particularly Q^0, Q^1, Q^2 and Q^3 which are finding similar to previous work on Si-NMR of silicate glasses [37]. Previous ^{29}Si-MAS-NMR work on commercial glasses found that the chemical shift experienced in bioactive glasses is related to the concentration of NBO and the neighbouring species. Stamboulis et al. found that increasing the number of NBO moves the peak in a positive direction while increasing the number of neighbouring Al atoms moves the peak in a negative direction. These findings are similar to the results achieved here, with the exception that chemical shift in this instance is less pronounced than previous studies [35].

The literature suggests that variations in the structural role of network intermediates such as Al^{3+} can influence the chemical and physical properties of silicate melts. The addition of alkali-metal cations to the glass (Na^+, Ca^{2+}) may influence the coordination state of the network intermediate (Al^{3+}, Ga^{3+}) which will determine its structural role in the glass [38]. In this context, understanding the role of Ga^{3+} in a bioactive glass can be beneficial as there is a

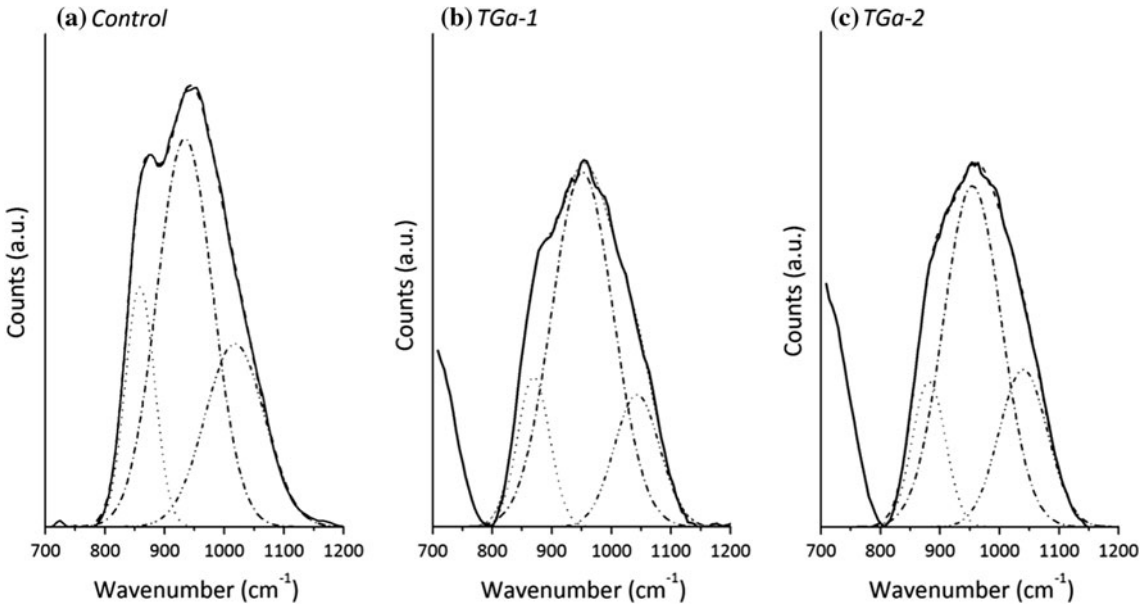

Fig. 6 Raman spectroscopy of Ga-glass series

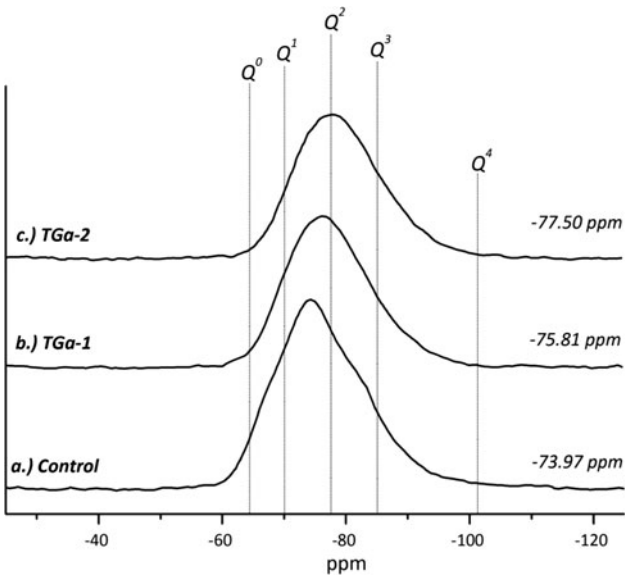

Fig. 7 MAS-NMR of Ga-glass series

greater degree of bioactivity associated with Ga^{3+} when compared to Al^{3+} [22, 39]. Studies on the structural role of Al^{3+} suggest that alkali ions acting as charge balancing agents up to an Al/*R* (*R* = any alkali) of 1.0, acts as a network former in fourfold coordination (AlO_4 tetrahedra). Surpassing an Al/*R* ratio of 1.0, the ions adopt a sixfold coordination state and act as a network modifier. Previous Raman studies by Condrate and co-workers [20] on Na_2O–Ga_2O_3–SiO_2 and K_2O–Ga_2O_3–SiO_2 glasses correlate a reduction in the NBO content of these glass compositions with an increase in Ga concentration as it enters the glass network in tetrahedral coordination. Regarding this study for *TGa-1* a Ga/*R* (*R* = Na) ratio of 0.8 is evident and for *TGa-2* the Ga/*R* concentration is 1.6. This suggests that a threshold level of Ga in tetrahedral formation may exist (Ga/*R* = 1.0), and above this limit, Ga may act as a network modifier. This suggests that at a Ga/*R* $\geq$ 1.0, Ga will assume a network modifying role and will subsequently be released from the glass in an aqueous environment, which can then provide a therapeutic benefit as a medical material. However, further ion release studies will need to be conducted in order to confirm this.

Conclusion

Bioactive glasses are characterised by their ability to release specific concentrations of therapeutic ions which is directly related to the structure of the glass and the concentration of NBOs present [17]. The results presented here, particularly NC, Raman and MAS-NMR, suggest that Ga predominantly acts as a network former in this glass series, however, a threshold level may exist where Ga adopts a network modifying role. Understanding the conditions where ions assume different coordination states can be important in order to further control glass dissolution and subsequently the ion release rate. Future work on these glasses will include ion release (ICP-OES, which will be correlated to glass structure) analysis testing with respect to particles size (<90 and ~425 μm). Also the therapeutic effect of Ga conducted in particular its effect on tumour cell proliferation using osteosarcoma cell lines.

Acknowledgement The authors would like to acknowledge Dr. Ulrike Werner-Zwanziger from the Department of chemistry at Dalhausie University for the acquisition of the ^{29}Si MAS-NMR data.

References

1. Hench LL (2006) J Mat Sci Mater Med 17:967
2. Vargas GE, Mesones RV, Bretcanu O, López JMP, Boccaccini AR, Gorustovich A (2009) Acta Biomater 5(1):374
3. Ochoa I, Sanz-Herrera JA, García-Aznar JM, Doblaré M, Yunos DM, Boccaccini AR (2009) J Biomech 42(3):257
4. Chen Q-Z, Rezwan K, Françon V, Armitage D, Nazhat SN, Jones FH, Boccaccini AR (2007) Acta Biomater 3(4):551
5. Chen QZ, Thompson ID, Boccaccini AR (2006) Biomaterials 27(11):2414
6. Cao B, Zhou D, Xue M, Li G, Yang W, Long Q, Ji L (2008) App Surf Sci 255(2):505
7. Day RM, Boccaccini AR, Shurey S, Roether JA, Forbes A, Hench LL, Gabe SM (2004) Biomaterials 25(27):5857
8. El-Kady AM, Ali AF, Farag MM (2010) Mat Sci Eng: C 30(1):120
9. Cannillo V, Chiellini F, Fabbri P, Sola A (2010) Comput Struct 92(8):1823
10. Brown RF, Day DE, Day TE, Jung S, Rahaman MN, Fu Q (2008) Acta Biomater 4(2):387
11. Valappil SP, Ready D, Abou Neel EA, Pickup DM, O'Dell LA, Chrzanowski W, Pratten J, Newport RJ, Smith ME, Wilson M, Knowles JC (2009) Acta Biomater 5(4):1198
12. da Silva JG, Azzolini LS, Wardell SMSV, Wardell JL, Beraldo H (2009) Polyhedron 28(11):2301
13. Kaneko Y, Thoendel M, Olakanmi O, Britigan BE, Singh PK (2007) J Clin Invest 117(4):877
14. Banin E, Lozinski A, Brady KM, Berenshtein E, Butterfield PW, Moshe M, Chevion M, Greenberg EP, Banin E (2008) Proc Natl Acad Sci USA 105(43):16761
15. Bastosa TO, Soares B, Cisalpino P, Mendesc I, dosSantosa R, Beraldoc H (2010) Microbio Res 165(7):573
16. Collery P, Keppler B, Madoulet C, Desoize B (2002) Critical Reviews Oncology/Hematology 42:283
17. Serra J, Gonzalez P, Liste S, Chiussi S, Leon B, Perez-amor M, Ylanen HO, Hupa M (2002) J Mater Sci Mater Med 13(12):1221
18. Kokubo T, Kim H-M, Kawashita M (2003) Biomaterials 24:2161
19. Kokubo T, Takadama H (2006) Biomaterials 27:2907
20. Higby PL, Shelby JE, Condrate RA (1986) J Non-Cryst Solids 84:93
21. Baker DR (1995) Geochim Cosmochim Acta 59(17):3561
22. Reusche E, Pilz P, Oberascher G, Linder B, Egensperger R, Gloeckner K, Trinka E, Iglseder B (2001) Hum Pathol 32(10):1136
23. Carter DH, Sloan P, Brook IM, Hatton PV (1997) Biomaterials 18:459
24. Boyd D, Towler MR, Watts S, Hill R, Wren AW, Clarkin OM (2008) J Mater Sci Mater Med 19:953
25. Mysen BO, Virgo D, Scarfe CM (1980) Am Miner 65:690
26. Deligkaris D, Tadele TS, Olthuis W, van den Berg A (2010) Sense Actuator B 147:765
27. Wang F, Li Z, Khan M, Tamama K, Kuppusamy P, Wagner WR, Sen CK, Guan J (2010) Acta Biomater 6(6):1978
28. Yildirim E, Dupree R (2004) Bull Mater Sci 27(3):269
29. Nicholson JW, Wilson AD (1993) Chemistry of solid state materials: acid-base cements–their biomedical and industrial applications. Cambridge University Press, Cambridge
30. Aguiar H, Serra J, Gonzalez P, Leon B (2009) J Non-Cryst Solids 335:475
31. Wren AW, Laffir FR, Kidari A, Towler MR (2010) J Non-Cryst Solids 357(3):1021
32. Gonzalez P, Serra J, Liste S, Chiussi S, Leon B, Perez-amor M (2003) J Non-Cryst Solid 320:92
33. McMillian PW (1984) Am Miner 69:622
34. Branda F, Arcobello-Varlese F, Costantini A, Luciani G (2002) Biomaterials 23:711
35. Stamboulis A, Law RV, Hill RG (2004) Biomaterials 25(17):3907
36. Parkinson BG, Holland D, Smith ME, Larson C, Doerr J, Affatigato M, Feller SA, Howes AP, Scales CR (2008) J Non-Cryst Solids 354:1936
37. Galliano PG, Porto JM, Spezl L, Varetti EL, Sobrados I, Sanz J (1994) Res Bull 29(12):1297
38. Mysen BO, Virgo D, Kushiro I (1981) Am Miner 66:678
39. Polizzi S, Pira E, Ferrara M, Bugiani M, Papaleo A, Albera R, Palmi S (2002) Neurotoxicology 23:761